RESEARCH ARTICLE

Electrophysiological Immunity to Plasmodiophora Brassicae Infection of Gaoshan Brassica Rapa under Various Selenite Levels

Antong Xia[1,2,*], Huakang Huang[1,2], Nan Mou[1,2], Jing Fan[1,2], Kun Zhai[1,2,*] and Dongshan Xiang[1,2]

[1] School of Chemical and Environmental Engineering, Hubei Minzu University, Enshi 445000, China
[2] Key Laboratory of Selenium Resource Research and Biological Application, Hubei Minzu University, Enshi 445000, China

Abstract

Enshi is a high-incidence area for *Plasmodiophora brassicae* infection in *Brassica rapa* in China; however, the differential immunomodulatory effects of selenite (Se^{4+}) on the infection of *Brassica rapa* by the *Plasmodiophora brassicae* (Pb) remain unclear. In this study, Enshi *Gaoshan Brassica rapa* (*GBr*) was selected. Pre-treatment with 0–10 mg/L Se^{4+} was applied, followed by artificial inoculation with *Plasmodiophora brassicae* spores (8×10^9 spore/mL). Growth characteristics, photosynthesis, and electrophysiological and nutritional metabolic features of *GBr* leaves were measured. The results indicate that electrophysiological techniques provide more significant distinctions. S2 (1.25 mg/L Se^{4+}) was identified as the optimal immune concentration. Compared to the CK, S2 exhibited a 1.2 fold increase in ΔG_r, a 19.5 fold increase in ΔG_z, and a 2.5 fold increase in Metabolic activity (MA). S4 (5 mg/L Se^{4+}) was the immune compensation concentration; compared to CK, S4 exhibited increased WRT (1.4 fold), Nutrient active translocation capacity (NAC) (1.9 fold), and ΔG (4 fold), achieving immune compensation. Therefore, electrophysiological indicators (ΔG_r, ΔG_z, MA, WRT, NAC) showed 30%–50% higher sensitivity than traditional photosynthetic parameters, highlighting the advantages of electrophysiological methods for early, non-destructive monitoring. This study provides innovative smart agricultural technical support for elucidating the immunity of differential Se^{4+}.

Keywords: *Plasmodiophora brassicae* infection, *Brassica rapa*, electrophysiological nutrient metabolism, immune regulation, health effects of selenium.

1 Introduction

Brassica rapa (Br) is a widely cultivated cruciferous vegetable that is vulnerable to Pb infection, which reduces cellular water content, impairs nutrient metabolism, and causes root deformities and plant death [1, 2]. In the past three years, clubroot infection in Br has caused global economic losses of up to 140 billion RMB [3]. Enshi, Hubei (108°23′12″ E to 110°38′08″ E, 29°07′10″ N to 31°24′13″ N) is a major production area for *GBr* in China, where clubroot

Submitted: 01 April 2026
Accepted: 29 May 2026
Published: 10 June 2026

Vol. 1, **No.** 2, 2026.
10.62762/JPE.2026.316376

***Corresponding authors:**
✉ Antong Xia
xiaantong@hbmzu.edu.cn
✉ Kun Zhai
zk3100@sina.com

Citation
Xia, A., Huang, H., Mou, N., Fan, J., Zhai, K., & Xiang, D. (2026). Electrophysiological Immunity to Plasmodiophora Brassicae Infection of Gaoshan Brassica Rapa under Various Selenite Levels. *Journal of Plant Electrobiology*, 1(2), 108–122.

disease poses a significant threat to cruciferous crop production [4]. Effective Pb control is essential for high-quality, high-yield production of highland *GBr*. Research indicates that exogenous selenium can modulate plant immune responses and stress resistance through transcriptomic and proteomic reprogramming [5], suggesting potential for Se^{4+} application in controlling Pb infection in Br. Se^{4+} improves resistance of Br by inhibiting fungal spore germination, disrupting cellulase activity [6], promoting Glutathione Peroxidase (GSH-Px) formation [7], and interacting with *Bacillus*-mediated selenium biosynthesis pathways [8]. Understanding the immunomodulatory effects of Se^{4+} is vital for efficient Pb infection management in Br.

Plant electrophysiological techniques are a reliable method for monitoring clubroot disease in *Brassica*. Based on plant electrophysiological techniques, Zhang et al. [9] investigated the intracellular electrophysiological water metabolism and nutrient transport thresholds in *Brassica napus* under low-phosphorus stress, enabling in situ monitoring of leaf water and nutrient use efficiency. Yu et al. [10] investigated whether electrophysiological parameters can substitute for growth and photosynthetic parameters to characterize the response of mulberry and paper mulberry to drought stress, providing a basis for water-saving smart management. Gu et al. [11] found that electrophysiological sensors reveal the silicon–selenium interaction on dynamic leaf intracellular water–nutrient metabolism in rice under cadmium stress, demonstrating that electrophysiological techniques can characterize multi-element interactions in plant stress responses. In the field of smart agricultural machinery, the "Plant Life Analyzer" and "Plant Membrane Function Analyzer" [12], developed based on plant electrophysiological technology, have garnered widespread acclaim from experts both domestically and internationally. The above findings indicate that plant electrophysiological technology provides a reliable method for elucidating the differential regulation of electrophysiological nutrient metabolism and immunity in *GBr* by Se^{4+} during Pb infection.

Wangying Town, Lichuan City (108.69° E, 30.27° N) is one of the primary areas in Enshi where Pb infection in highland Br is prevalent, as the local soil chemical and microbial characteristics are conducive to clubroot disease development [13]. Studies have shown that the peak incidence of Pb infection in Chinese cabbage typically occurs from August to September [14], with optimal temperatures for disease development ranging from 25–30°C [15], and the disease primarily affecting the seedling stage (2–3 leaf stage) [16], with the optimal disease resistance window not exceeding 10 days [17]. The research team previously determined that the immunity threshold for GBr against Pb is 8×10^9 cells/mL [18].

In summary, this study collected clubroot pathogen samples and healthy GBr seedlings from Wangying Town, Lichuan City. Using a substrate culture (sphagnum peat : vermiculite volume ratio is 2:1), the following experiments were conducted: acclimation (7 days), Se^{4+} intervention prior to Pb infection (10 days), and artificial inoculation with Pb (10 days). We measured GBr growth characteristics, photosynthesis, and electrophysiological and nutritional metabolic features, including GBr metabolic activity (MA) and average metabolic energy (ΔG). Based on correlation analysis (ANOVA) and principal component analysis (PCA), this study elucidated the differential immune regulation of Se^{4+} concentrations on Pb infection in GBr, providing innovative smart agricultural technology to uncover the mechanisms of Se^{4+} mediated immune regulation.

2 Materials and Methods

2.1 Collecting *Pb* infected and healthy *GBr* seedlings

On August 31, 2025, *Pb* tissues and healthy *GBr* plants were collected from Sujiaqiao Village, Wangying Town, Lichuan City. The *Pb* tissues and root systems of the healthy *GBr* plants were soaked in tap water, stored in foam boxes, and transported to the laboratory for later use. The *Pb* tissues were stored in a freezer at -20°C.

2.2 Experimental Procedures

2.2.1 GBr seeding cultivation

From Sept. 1^{st} to 7^{th} (7 day), *GBr* acclimatization cultivation experiments were conducted using a substrate medium (sphagnum peat : vermiculite volume ratio = 2:1). *GBr* seedlings were watered with a 1/2-strength Hogland nutrient solution, formulated as follows: KNO_3: 2.5 mM, $NH_4H_2PO_4$: 1.0 mM, $Ca(NO_3)_2 \cdot 4H_2O$: 2.5 mM, $MgSO_4 \cdot 7H_2O$: 1.0 mM, H_3BO_3: 23.1 μM, $CuSO_4 \cdot 5H_2O$: 0.16 μM, $ZnSO_4 \cdot 7H_2O$: 0.38 μM, $MnCl_2 \cdot 4H_2O$: 4.55 μM, $Na_2MoO_4 \cdot 2H_2O$: 0.19 μM, Fe-EDTA: 50 μM [19].

2.2.2 Prior different Se^{4+} treatment

From Sept. 8^{th} to 18^{th} (10 day), various Se^{4+} intervention treatments were applied prior to Pb

infection of *GBr*. Referring to the Se^{4+} safety thresholds for Brassicaceae plants [20], a root-applied method was selected, and *GBr* seedlings were treated with different concentrations of Se^{4+} (Na_2SeO_3, analytical purity ≥98%) via root application: Ck (0 mg/L Se^{4+}), S1 (0.625 mg/L Se^{4+}), S2 (1.25 mg/L Se^{4+}), S3 (2.5 mg/L Se^{4+}), S4 (5 mg/L Se^{4+}), S5 (10 mg/L Se^{4+}).

2.2.3 *Pb infection experiment*

From September 19th to 29th, 50 g of Pb nematode samples were collected and allowed to thaw naturally at room temperature (25°C). The Pb nematode sample was disrupted using a cell disruptor, mixed with 250 mL of sterile water, and ground. The mixture was then filtered through eight layers of sterile medical gauze. The filtered bacterial suspension was diluted 100-fold using a pipette, stained with 200× aniline blue, and the concentration was determined using the hemocytometer method. The suspension was diluted to 8×10^9 cells/mL and stored at 4°C for later use. Artificial inoculation of Pb was performed [12] by withdrawing 1 mL of bacterial suspension and injecting it into the root of *GBr*, ensuring the suspension flowed evenly to the base of the taproot. The inoculation period was 10 days. For each treatment, 12 plants were selected, and 3 *GBr* seedlings with consistent growth were chosen for tests of growth characteristics, photosynthesis, and plant electrophysiology.

2.3 Growth Characteristics

2.3.1 *Biomass*

After harvest, following the method described in research [21], roots, stems, and leaves were collected from *GBr* plants subjected to different Se^{4+} treatments, and the fresh weight (FW, g/plant) was determined using a balance (0.0001 g, AR124CN, Shanghai, China).

2.3.2 *Total Chlorophyll and Total Nitrogen Content*

A chlorophyll meter (0–99.9 SPAD, IN-YL03, Shandong, China) was used to measure the total chlorophyll and total nitrogen content in *GBr*, following established SPAD-based assessment methods for vegetable nitrogen nutritional status [22].

2.4 Photosynthesis

Fully expanded leaves from the second leaflet of *GBr* were selected. A Li-6400 portable photosynthetic meter (LI-COR, Lincoln, NE, USA) was used to measure photosynthetic parameters of *GBr*, including Pn, Gs, Ci, and Tr, following standard Li-6400 measurement procedures applied in vegetable crop research [23], including: net photosynthetic rate (Pn), stomatal

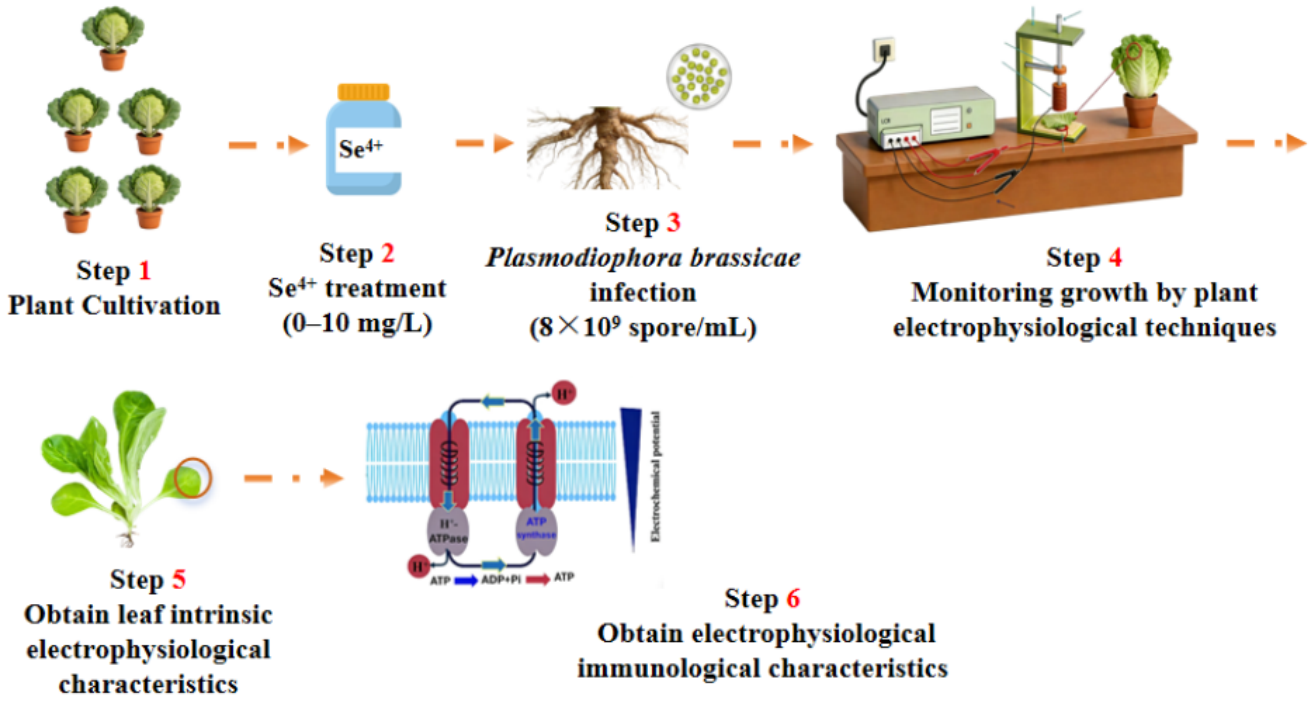

Figure 1. Flowchart of the experimental procedure.

conductance (Gs), intercellular CO_2 concentration (Ci), and transpiration rate (Tr).

2.5 Intrinsic leaf Electrophysiological Characteristics

Following the method described in research [12], the capacitance (Cp), resistance (R), and impedance (Z) of the *GBr* electrode were measured (Figure 1). Electrophysiological models were then constructed for these three electrical signals as a function of different clamping forces (F, force; F = 1–7 N, with one measurement per 1 N increment), as shown in Formulas (1–4). Here, F is the applied clamping force, in N; M is the mass of the iron block; m is the total mass of the plastic rod and electrode plate, in kg; g is the acceleration due to gravity, taken as 9.8 N/kg; x_0, y_0, and p_0 are the intercepts of the fitting equations for the *GBr* blade's capacitance C, resistance R, and impedance Z versus clamping force F, respectively; h, k_1, and k_2 are the independent variable coefficients in the fitting equation for the *GBr* blade capacitance (Cp), resistance (R), and impedance (Z) versus the clamping force (F), respectively; b_1 and b_2 are the power exponent coefficients in the fitting equation for Cp, R, and Z versus F, respectively. Otherwise, capacitive reaction (X_C): Plant tissue is equivalent to a biological capacitor, characterizing the charge storage and rapid charge-discharge capacity of cell membranes, which showed in formula 5. Inductive reaction (X_L): Plant tissue is equivalent to a biological inductor, characterizing the inertial response of intracellular ion flow and bioelectricity, which showed in formula 7.

$$F = (M + m)g \tag{1}$$
$$Cp = x_0 + hF \tag{2}$$
$$R = y_0 + k_1 e^{-b_1 F} \tag{3}$$
$$Z = p_0 + k_2 e^{-b_2 F} \tag{4}$$

Based on the *GBr* blade's Cp, the physiological capacitive reactance (X_c) and the model relating X_c to F are given in Formulas 5–6. Based on the *GBr* blade's Z, R, and X_c, the physiological inductive reactance (X_L) and the model describing how X_L varies with F are calculated, as shown in Formulas 7–8. Here, $\pi = 3.14$; $f = 1.5$ kHz; q_0, k_3, and b_3 are the intercept, independent variable coefficient, and power-law coefficient of the fitting equation for X_c versus F for the *GBr* blade, respectively. a_0, k_4, and b_4 are the intercept, independent variable coefficient, and the fitting equation for X_L versus F, respectively.

$$X_c = \frac{1}{2\pi f C_p} \tag{5}$$
$$X_c = q_0 + k_3 e^{-b_3 F} \tag{6}$$
$$\frac{1}{-X_L} = \frac{1}{Z} - \frac{1}{R} - \frac{1}{X_c} \tag{7}$$
$$X_L = a_0 + k_4 e^{-b_4 F} \tag{8}$$

When $F = 0$, based on Formulas (3), (6), and (8), quantify the *GBr* blade's intrinsic capacitance (I_{Cp}), intrinsic resistance (I_R), intrinsic capacitive reactance (I_{Xc}), intrinsic inductive reactance (I_{XL}), and intrinsic impedance (I_Z), as shown in Formulas 9–13.

$$I_{Cp} = \frac{1}{2\pi f X_L} \tag{9}$$
$$I_R = y_0 + k_1 \tag{10}$$
$$I_{Xc} = q_0 + k_3 \tag{11}$$
$$I_{XL} = a_0 + k_4 \tag{12}$$
$$\frac{1}{I_Z} = \frac{1}{I_R} + \frac{1}{I_{Xc}} - \frac{1}{I_{XL}} \tag{13}$$

2.6 Leaf electrophysiological water metabolism

The leaf intracellular water holding capacity (IWHC), leaf effective thickness (d), intracellular water use efficiency (IWUE), intracellular water holding time (IWHT) and water transfer rate (WRT), as shown in formulas 14-18, U is 1.5 V, h is the independent variable coefficient in the equation fitting C and F.

$$IWHC = \sqrt{ICp^3} \tag{14}$$
$$d = \frac{U^2 h}{2} \tag{15}$$
$$IWUE = \frac{d}{IWHC} \tag{16}$$
$$IWHT = Cp \times Z \tag{17}$$
$$WRT = \frac{IWHC}{IWHT} \tag{18}$$

2.7 Electrophysiological Metabolic Activity

The relative metabolic flux (MF), relative metabolic rate (MR), and relative metabolic activity (MA) of *GBr* leaves are given in Formulas (24–26). Here, MA represents the electrophysiological metabolic activity of *GBr*, a higher MA indicates a lower degree of *Pb* infection and more vigorous growth.

Table 1. Biomass of *Pb*-contaminated *GBr* roots, stems, and leaves under different Se^{4+} treatments. FW is clearly defined as fresh weight per plant. Data are presented as: mean ± standard error; different lowercase letters (a–e) indicate significant differences (n = 3, $p < 0.05$).

Groups	CK	S1	S2	S3	S4	S5
Root (FW, 10^1 g/plant)$_0$	$5.6 \pm 0.2e_0$	$10.7 \pm 0.5b_0$	$15.9 \pm 0.1a_0$	$14.9 \pm 0.3a_0$	$10.6 \pm 0.26c_0$	$4.6 \pm 0.27d_0$
Stem (FW, 10^1 g/plant)$_0$	$30.6 \pm 03d_0$	$47.1 \pm 4b_0$	$118.8 \pm 2a_0$	$111.8 \pm 2a_0$	$33.9 \pm 1c_0$	$31.4 \pm 1d_0$
Leaves (FW, 10^1 g/plant)$_0$	$36.3 \pm 5d_0$	$58 \pm 3b_0$	$122.2 \pm 2a_0$	$126.9 \pm 3a_0$	$45 \pm 1c_0$	$36.4 \pm 1d_0$

Table 2. Total chlorophyll and total nitrogen content in *Pb*-contaminated *GBr* leaves under different Se^{4+} treatments. Data are presented as: mean ± standard error; different lowercase letters a–c indicate significant differences (n = 3, $p < 0.05$).

Groups	CK	S1	S2	S3	S4	S5
Total chlorophyll content (mg/g)	$37.2 \pm 0.53c$	$38.63 \pm 1.04b$	$38.73 \pm 0.75a$	$41.23 \pm 0.95a$	$42.3 \pm 0.52a$	$42.3 \pm 0.52a$
Total nitrogen content (mg/g)	$14.43 \pm 0.21c$	$14.83 \pm 0.35b$	$14.93 \pm 0.25a$	$15.7 \pm 0.3a$	$16.03 \pm 0.12a$	$15.27 \pm 0.35a$

$$MF = \frac{1}{\mathrm{IR} \times \mathrm{IZ} \times \mathrm{IX}_C \times \mathrm{IX}_L} \tag{24}$$

$$MR = \mathrm{WRT} \times \mathrm{NAC} \tag{25}$$

$$MA = \sqrt[6]{\mathrm{MF} \times \mathrm{MR}} \tag{26}$$

2.8 Cellular metabolic characteristics Based on IR and IZ

The electrophysiological metabolic energy, unit metabolic energy, and total metabolic energy based on IR and IZ are denoted as ΔG_{RE} (the unit for the metabolizable energy of leaf cells) and ΔG_{ZE} (Z-based metabolic energy per unit of plant leaf cells), respectively; see Formulas 27-28; ΔG_R (cell metabolic energy based on the intrinsic resistance of the leaf), ΔG_Z (cell metabolic energy based on the intrinsic impedance of leaves), and ΔG (average metabolic energy), as shown in Formulas 29-31. $\ln k_2$ is the natural logarithm of the rate constant k_2, $\ln p_0$ is the natural logarithm of the initial parameter p_0, and b_2 is the metabolic energy coefficient.

$$\Delta G_{RE} = \frac{\ln k_1 - \ln y_0}{b_1} \tag{27}$$

$$\Delta G_{ZE} = \frac{\ln k_2 - \ln p_0}{b_2} \tag{28}$$

$$\Delta G_R = \Delta G_{RE} \times d \tag{29}$$

$$\Delta G_Z = \Delta G_{ZE} \times d \tag{30}$$

$$\Delta G = \frac{\Delta G_R + \Delta G_Z}{2} \tag{31}$$

2.9 Statistical Analysis

SigmaPlot 15.0 was used to fit the *GBr* electrophysiological equations; SPSS 27.0 was used to perform statistical tests for significant differences in the data, with different letters (a–f) indicating significant differences between data points. Results are expressed as "mean ± standard deviation"; SPSS 21 was used to perform one-way analysis of variance (ANOVA) and the least significant difference (LSD) test ($p < 0.05$), while Origin 2025 was used to generate correlation heatmaps and PCA analysis.

3 Results

3.1 Growth Characteristics

Figure 2 shows the phenotypic characteristics of Pb-infected *GBr* under different treatments. Table 1 presents the root, stem, and leaf biomass of *GBr*, while Table 2 shows the total chlorophyll and total nitrogen content of *GBr*. Treatments S1–S5 all promoted the fresh weight of roots, stems, and leaves, as well as the total chlorophyll and total nitrogen content of Pb-infected *GBr*, with S2 and S3 exhibiting the most significant effects. S2 exhibited the highest root, stem, and leaf biomass, with root, stem, and leaf fresh weight increased by approximately 1.84-, 2.88-, and 2.37-fold over CK, respectively. S3 had the highest chlorophyll and total nitrogen content (Table 2), increasing by 10.8% and 8.7%, respectively, compared to CK. Overall, there were no significant differences in growth characteristics between S2 and

Table 3. Intracellular electrophysiological water metabolism and nutrient transport characteristics in *Pb*-stressed *GBr* leaves under different Se^{4+} treatments. Data are presented as mean ± standard error; different lowercase letters a–f indicate significant differences among groups ($n = 3$, $p < 0.05$).

Groups	CK	S1	S2	S3	S4	S5
IWHC (10^3)	$1.32 \pm 0.0052e_4$	$2.69 \pm 0.003b_4$	$3.32 \pm 0.038a_4$	$2.22 \pm 0.033c_4$	$2.26 \pm 0.025c_4$	$1.52 \pm 0.026d_4$
IWUE	$7.97 \pm 0.06e_4$	$4.68 \pm 0.57f_4$	$16.37 \pm 0.36b_4$	$11.73 \pm 0.31d_4$	$13.6 \pm 0.17c_4$	$17.47 \pm 0.276a_4$
IWHT	$36.66 \pm 0.15a_4$	$33 \pm 0.26a_4$	$26.93 \pm 0.18bc_4$	$16.52 \pm 0.51d_4$	$26.31 \pm 2.18c_4$	$28.37 \pm 0.19b_4$
WRT (10^3)	$0.36 \pm 0.001e_4$	$0.816 \pm 0.006c_4$	$1.23 \pm 0.01b_4$	$1.84 \pm 0.003a_4$	$0.86 \pm 0.07c_4$	$0.53 \pm 0.005d_4$
UNF	$1.55 \pm 0.01b_4$	$2.01 \pm 0.02a_4$	$1.16 \pm 0.01c_4$	$0.52 \pm 0.01e_4$	$1.01 \pm 0.09d_4$	$1.08 \pm 0.01d_4$
NTR (10^3)	$0.36 \pm 0.001e_4$	$0.816 \pm 0.006c_4$	$1.23 \pm 0.009b_4$	$1.84 \pm 0.003a_4$	$0.86 \pm 0.07c_4$	$0.53 \pm 0.005d_4$
NTC (10^3)	$0.055 \pm 0.003e_4$	$1.64 \pm 0.021a_4$	$1.44 \pm 0.018b_4$	$0.70 \pm 0.009d_4$	$0.87 \pm 0.012c_4$	$0.58 \pm 0.011e_4$
UAF	$0.6 \pm 0.03c_4$	$0.45 \pm 0.04e_4$	$0.71 \pm 0.03b_4$	$0.5 \pm 0.01d_4$	$0.74 \pm 0.02a_4$	$0.71 \pm 0.01b_4$
NAC (10^3)	$0.21 \pm 0.001d_4$	$0.37 \pm 0.003c_4$	$0.88 \pm 0.004a_4$	$0.68 \pm 0.029b_4$	$0.64 \pm 0.076b_4$	$0.38 \pm 0.002c_4$

S3.

3.2 Photosynthesis

Figure 3 illustrates the photosynthetic performance of *Pb*-infected *GBr* under different Se^{4+} treatments. All treatments S1–S5 enhanced the net photosynthetic rate (Pn; Figure 3(a)), stomatal conductance (Cond; Figure 3(c)), and transpiration (Tr; Figure 3(d)) in *Pb*-infected *GBr*, while reducing intercellular gas (Ci, Figure 3(b)). The S2 and S3 treatments exhibited the most significant promotion of Pn, Cond, and Tr, as well as the most pronounced suppression of Ci. Taking S2 as an example, compared to CK, S2 showed increases in Pn, Cond, and Tr of 65.1%, 2.8-fold, and 1.5-fold, respectively, while Ci decreased by 26.8%. However, overall, there was no significant difference in photosynthesis between S2 and S3.

3.3 Electrophysiological Fitting Equations for *GBr* Leaves

Figure 4 shows the electrophysiological equations for capacitance (Cp, Figure 4(a)), resistance (R, Figure 4(b)), impedance (Z, Figure 4(c)), physiological reactance (X_C, Figure 4(d)), and physiological capacitive reactance (X_L, Figure 4(e)) of Pb-infected *GBr* leaves under different Se^{4+} treatments, as a function of clamping force F (1–7 N). The results show that the electrophysiological equations for Cp, R, Z, X_C, and X_L of *GBr* are significantly correlated with F (R^2 = 0.98–0.99), and there are significant differences among the electrophysiological equations of S1–S5 ($p < 0.01$).

3.4 Intrinsic Electrophysiological Parameters of *GBr* Blades

Figure 5 shows the intrinsic electrophysiological parameters of *GBr* blades, including: ICp (Figure 5(a)), IR (Figure 5(b)), IZ (Figure 5(c)), IX_c (Figure 5(d)), and IX_L (Figure 5(e)). The results show that S1–S5 all increased ICp and decreased IR, IZ, IX_c, and IX_L. Compared to CK, the changes in S2 were the most significant: ICp in S2 increased threefold, while IR, IZ, IX_c, and IX_L decreased by 83.3%, 81.6%, 74.9%, and 78.6%, respectively.

3.5 Electrophysiological Water Metabolism and Nutrient Transport Capacities of *GBr* Leaves

Table 3 shows the electrophysiological water metabolism (IWHC, IWUE, IWHT, and WTR) and nutrient transport (UNF, NTR, NTC, UAF, and NAC) characteristics of *GBr* leaves infected with *Pb* under different Se^{4+} treatments. As Se^{4+} concentration increased, IWHC, IWUE, and WTR in electrophysiological water metabolism initially increased and then decreased, while IWHT showed the opposite trend. S2 exhibited the highest IWHC and IWUE, which were 1.5-fold and 1.05-fold higher than CK, respectively. S5 exhibited the lowest IWHT, which was 54.9% lower than CK. In electrophysiological nutrient transport, NTR, NTC, UAF, and NAC showed a trend of initially increasing and then decreasing. S2 exhibited the highest NAC, which was approximately 4.2 times higher than CK; S3 exhibited the lowest UNF, which was 66.3% lower than CK.

3.6 Electrophysiological and Metabolic Characteristics of *GBr* Leaves

Figure 6 shows the electrophysiological and metabolic characteristics of *Pb* infected *GBr* leaves under different Se^{4+} treatments. As Se^{4+} concentration increased, MF, MR, and MA initially increased and then decreased. S2 exhibited the highest MF and MA values, which were 101-fold and 2.5-fold higher than those of CK, respectively.

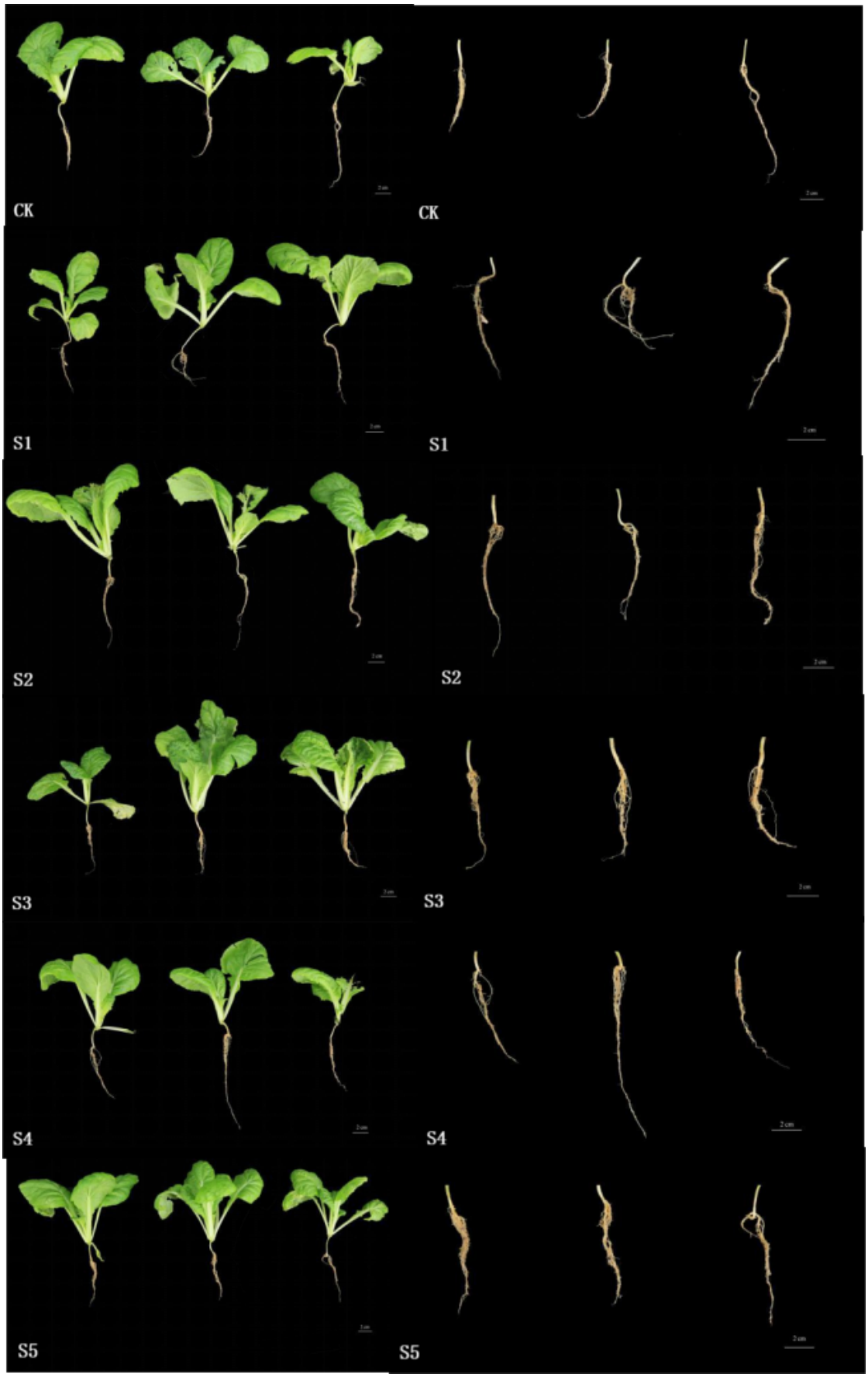

Figure 2. Phenotypic characteristics of Pb stressed GBr plants and roots under different treatments. CK (0 mg/L Se^{4+}), S1 (0.625 mg/L Se^{4+}), S2 (1.25 mg/L Se^{4+}), S3 (2.5 mg/L Se^{4+}), S4 (5 mg/L Se^{4+}), S5 (10 mg/L Se^{4+}). The concentration of Pb infection used was 8×10^9 spores/mL.

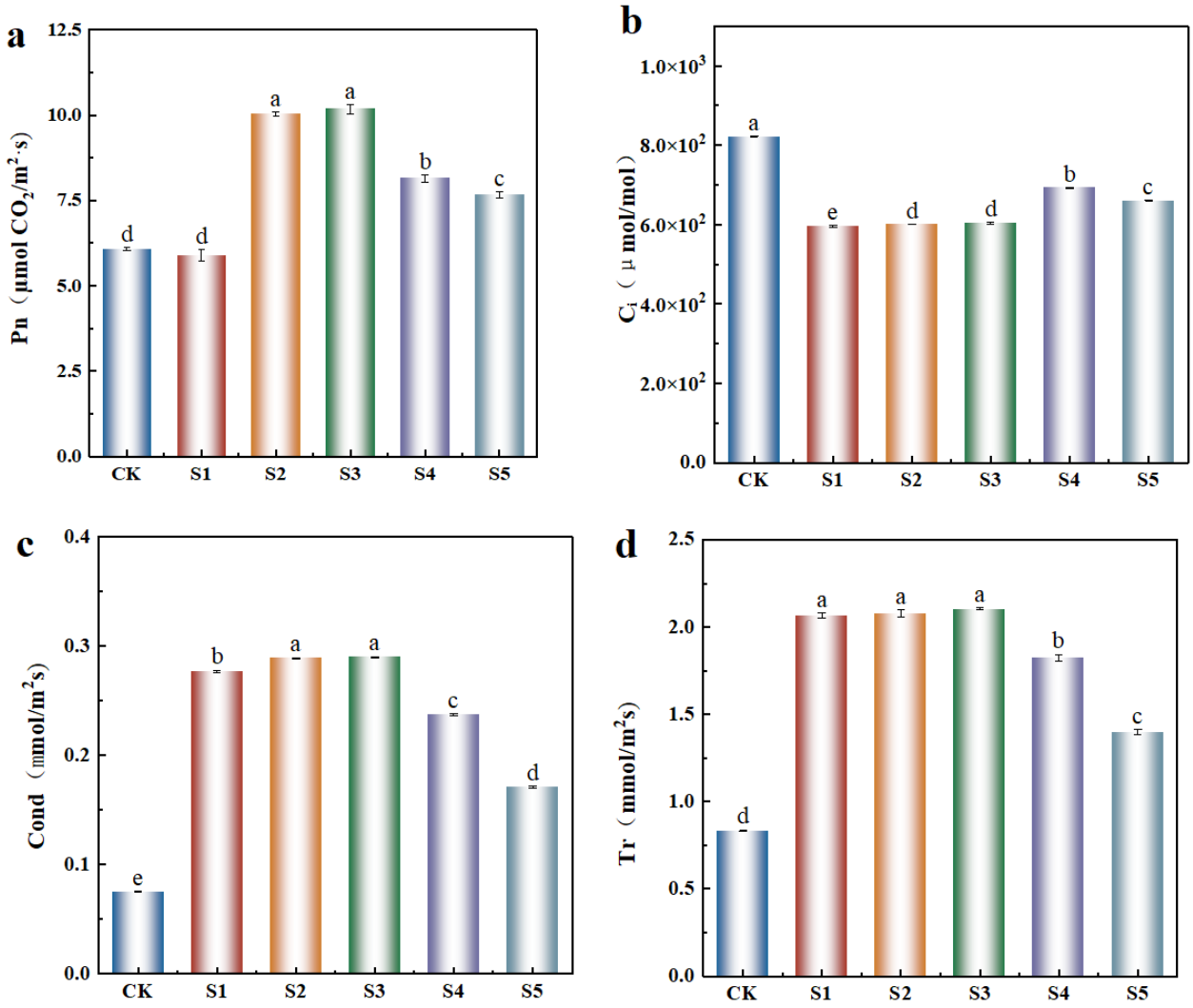

Figure 3. Effects of different Se^{4+} treatments on photosynthesis in Pb-stressed GBr. (a) Net photosynthetic rate (Pn); (b) Intercellular CO_2 concentration (Ci); (c) Stomatal conductance (Cond); (d) Transpiration rate (Tr). Data are presented as mean ± standard error; different lowercase letters a–e indicate significant differences ($n = 3$, $p < 0.05$).

3.7 Cellular Metabolic Energy in the IR and IZ of *GBr* Leaves

Figure 7 shows the cellular metabolic energy in the IR and IZ of *GBr* leaves infected with *Pb* under different Se^{4+} treatments, based on the specific metabolic energy of the IR (ΔG_R) and IZ (ΔG_Z) as well as the total cellular metabolic energy (ΔG). As Se^{4+} concentration increased, ΔG_R, ΔG_Z, and ΔG initially increased and then decreased. S2 exhibited the highest values for ΔG_R, ΔG_Z, and ΔG, which were 1.2, 19.5, and 18.1 times higher than those of CK, respectively.

3.8 ANOVA and PCA

Figure 8 shows the correlation analysis (Figure 8(a)) and principal component analysis (Figure 8(b)) of the electrophysiological and nutritional metabolic characteristics of *GBr* leaves under different Se^{4+} treatments. The results of Figure 8(a) indicate that *GBr*'s MA is significantly positively correlated with WRT, NTR, NAC, MF, and MR, and significantly negatively correlated with IR and IZ. Figure 8(b) shows that PC1 accounts for 81.4% of the variance, while PC2 accounts for 10.9%. The principal factors for S1–S5 are as follows: S1 consists of IR and IZ; S2 consists of MF; S3 consists of MR; S4 consists of NAC, WRT, and NTR; and S5 is identical to S1, consisting of IR and IZ.

4 Discussion

4.1 Advantages of In Situ Monitoring Using Plant Electrophysiological Techniques

Under Pb infection, 0.625–5 mg/L Se^{4+} significantly promoted the growth of *GBr*, as evidenced by increased biomass (Figure 2, Tables 1 and 2) and photosynthesis (Figure 3) in S1–S4. However, compared to CK, there were no significant differences

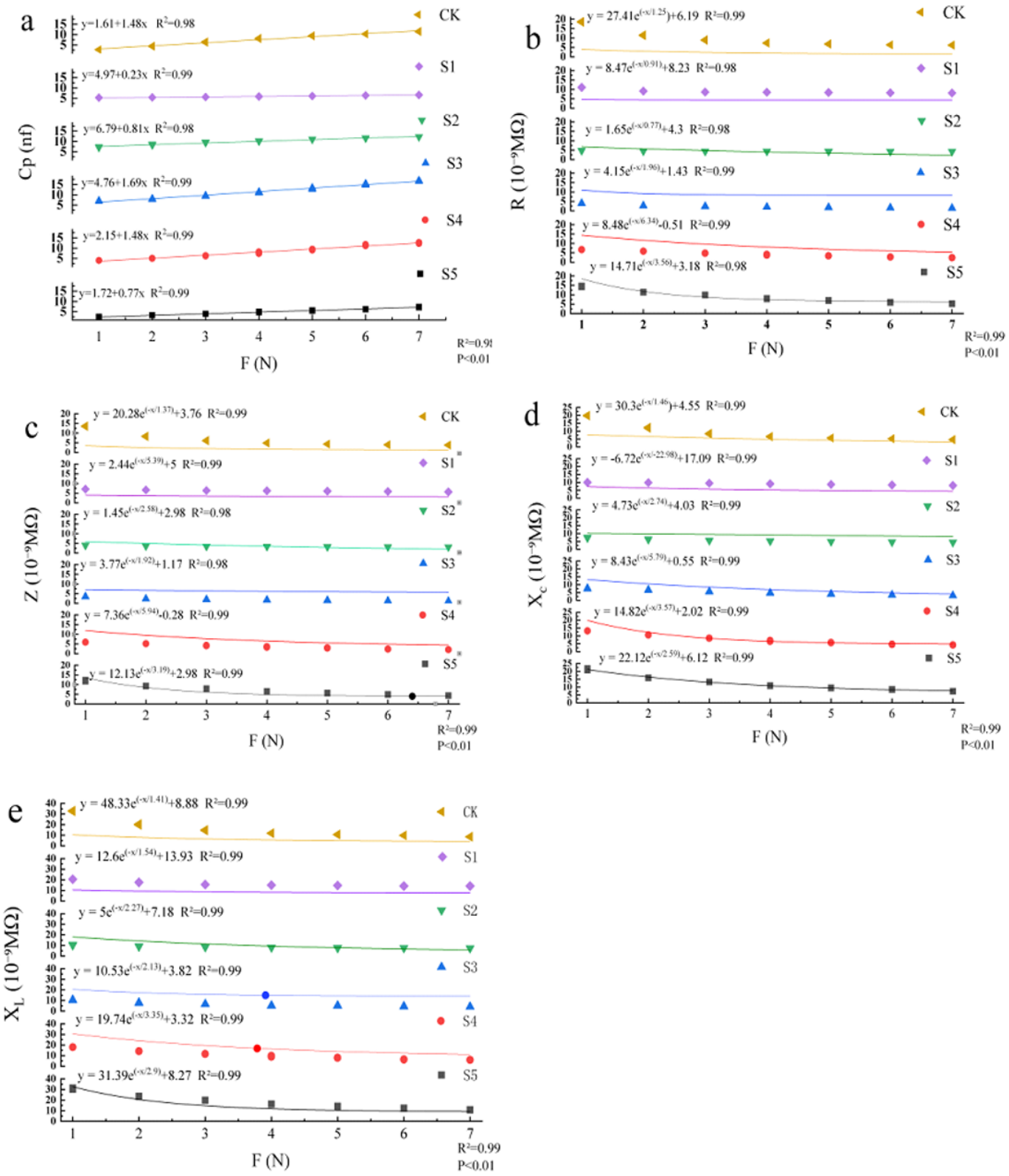

Figure 4. Fitting equations for Pb-induced changes in *GBr* leaf electrophysiological parameters under different Se^{4+} treatments versus clamping force (F = 1–7 N). (a) Capacitance (Cp); (b) Resistance (R); (c) Impedance (Z); (d) Physiological reactance (X_C); (e) Physiological inductive reactance (X_L). Data are presented as mean ± standard error ($n = 3$, $R^2 = 0.98$–0.99, $p < 0.01$).

in growth characteristics and photosynthesis between S2 and S3, plant electrophysiological techniques further distinguished their immunological differences. In the electrophysiological equations for *GBr*'s Cp,

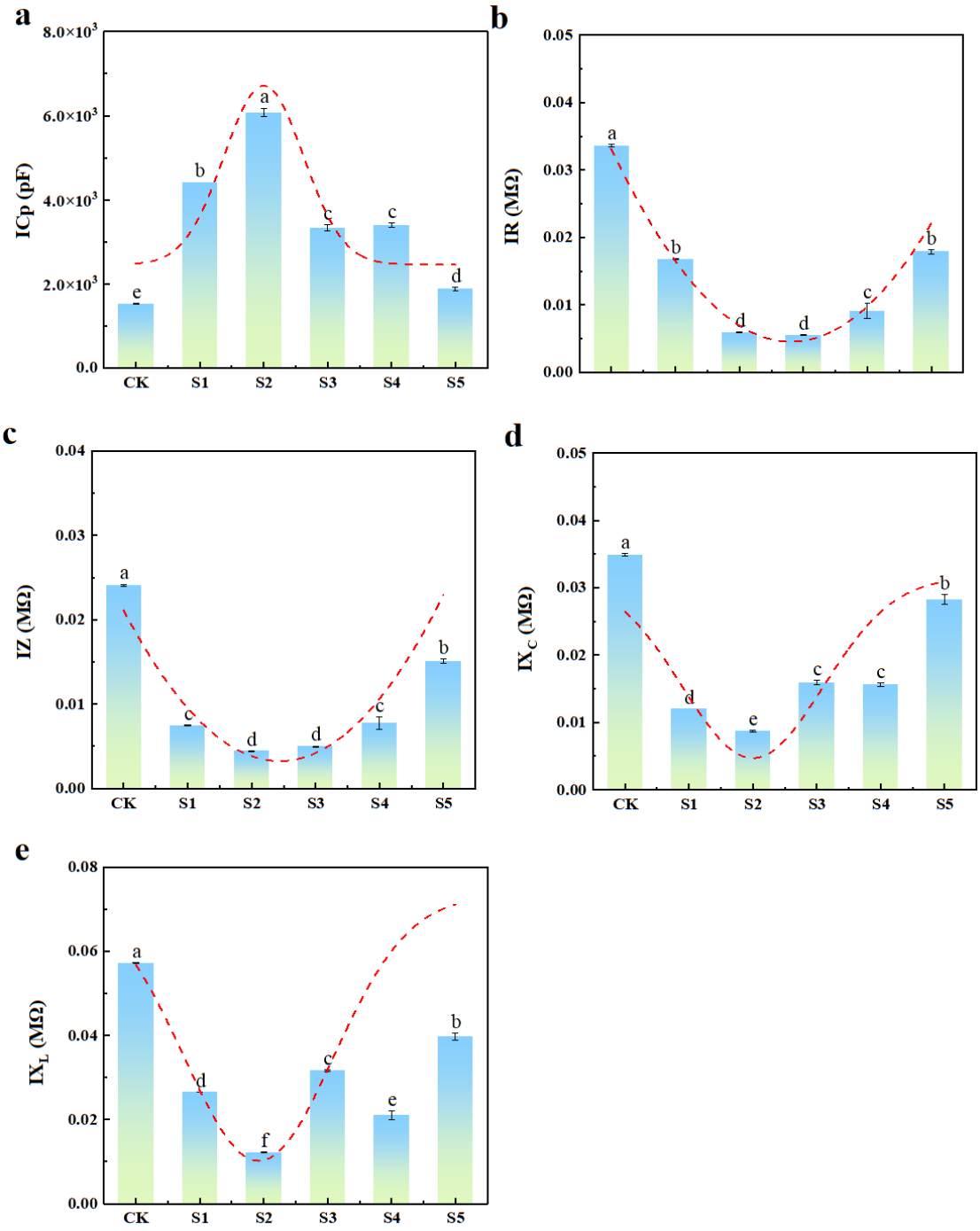

Figure 5. Leaf inherent electrophysiological characteristics of Pb-infected *GBr* under different Se^{4+} treatments. (a) Inherent capacitance (ICp); (b) Inherent resistance (IR); (c) Inherent impedance (IZ); (d) Inherent physiological reactance (IX_C); (e) Inherent physiological inductive reactance (IX_L). Data in the figure are presented as mean ± standard error; different lowercase letters a–f indicate significant differences among groups ($n = 3$, $p < 0.05$).

R, Z, X_C and X_L versus F ($p < 0.01$, Figure 4) indicates that there are significant differences in the electrophysiological parameters of *GBr* under different Se^{4+} concentrations, consistent with the concentration-dependent metabolic reprogramming observed in selenium-treated Brassicaceae plants [24]. R^2 values ranged from 0.98 to 0.99, indicating the reliability of the electrophysiological equations. Studies have shown that leaf intrinsic capacitance is positively correlated with plant growth vigor [12], while intrinsic resistance, impedance, physiological capacitance, and physiological reactance are negatively correlated with plant growth vigor [25]. The higher the IC_P and the lower the IX_C and IX_L values in S2, the greater the growth-promoting effect of S2 on *GBr*. In summary, S2 (1.25 mg/L) is the optimal immune

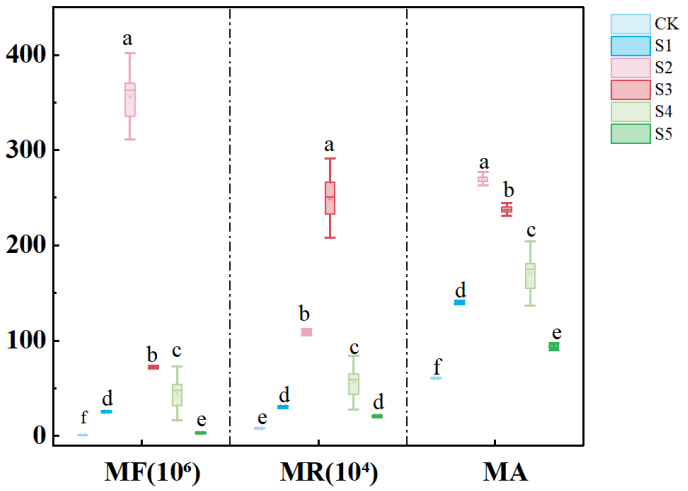

Figure 6. Electrophysiological and metabolic characteristics of *Pb* stressed *GBr* leaves under different Se^{4+} treatments, from left to right: MF, MR, and MA. Data are presented as mean ± standard error; significant differences between groups are indicated by lowercase letters a–f (n = 3, p < 0.05).

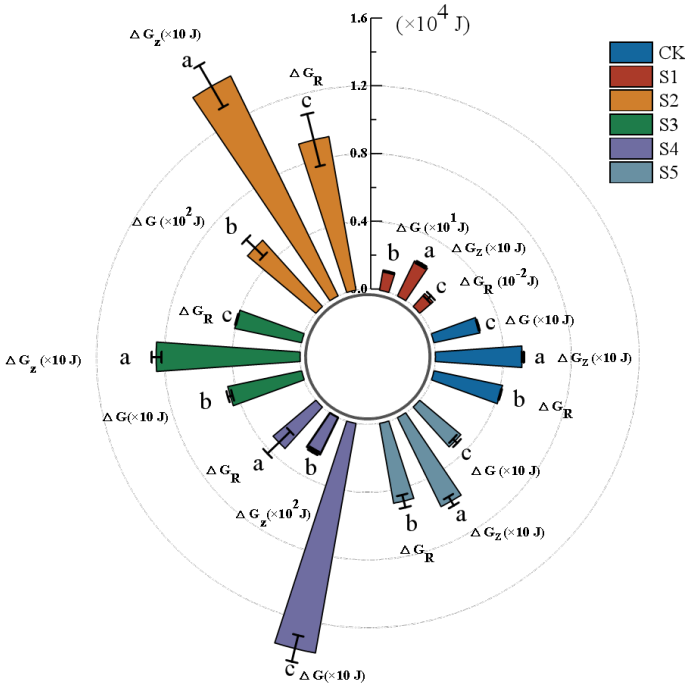

Figure 7. Unit cell metabolic energy (ΔG_R) and total cell metabolic energy (ΔG) in the IR (ΔG_R) and IZ (ΔG_Z) regions of Pb-stressed *GBr* leaves under different Se^{4+} treatments. Data are presented as mean ± standard error; different lowercase letters (a–c) indicate significant differences among groups ($n = 3, p < 0.05$).

concentration for preventing Pb infection in *GBr*.

4.2 Electrophysiological Characteristics of Water and Nutrient Metabolism Differences in *GBr* Leaves Mediated by Se^{4+} During *Pb* Infection

In this study, under Pb infection, Se^{4+} significantly promoted Cond (Figure 3(c)) and Tr (Figure 3(d)) in *GBr*, indicating that Se^{4+} participates in the regulation of water metabolism in *GBr* mesophyll cells [26]. S2 (1.25 mg/L Se^{4+}) was the optimal immunity concentration for controlling Pb infection in *GBr*. Electrophysiological water metabolism analysis showed that in the S2 treatment, IWHC and IWUE increased, while IWHT decreased. Electrophysiological nutrient transport characteristics indicated that the S2 treatment exhibited the highest NAC and the lowest UNF (Table 3). Studies have shown that a plant's net photosynthetic rate is positively correlated with cellular water-holding capacity and active nutrient transport capacity [27], and negatively correlated with water movement rate and passive nutrient transport capacity [28], indicating that S2 enhances *GBr* resistance to Pb infection by prolonging the water-holding duration and improving water utilization efficiency, increasing active nutrient transport capacity [29], and promoting Pn (Figure 3(a)) and MA (Figure 6) in S2, exhibited the highest values for ΔG_R, ΔG_Z, and ΔG (Figure 7), attributed to S2's promotion of water metabolism and active nutrient transport in *GBr* leaf cells infected by the root-knot nematode [30], which facilitated the synthesis of chlorophyll and total nitrogen (Table 2) [31, 32] and enhanced *GBr* cellular metabolic activity. Additionally, the ΔG_R and ΔG_Z values in S4 did not decrease linearly but instead increased slightly, though they remained lower than those in S2, indicating that S4 triggered immune compensatory metabolism in *GBr* [33]. However, at S5 (10 mg/L Se^{4+}), the promoting effect of Se^{4+} diminished, as evidenced by the following: IWUE was highest at S5, while IWHC and WRT were significantly reduced, and NTC and NAC decreased, resulting in both MA and Pn being lower than those at S2. ΔG_R and ΔG_Z values at S5 continued to decline, indicating that the immune compensation observed at S4 was short-lived [34], as reflected in the continued decline in growth at S5. In summary, S4 (5 mg/L Se^{4+}) is the concentration that prevents immune compensation in Pb infection of *GBr*. The transient effect is mainly due to the assimilation and immobilization of exogenous Se^{4+} in plant species. Repeated application and synergy with Pb infection can prolong the efficacy by improving Se utilization and maintaining sustained immune activation [33].

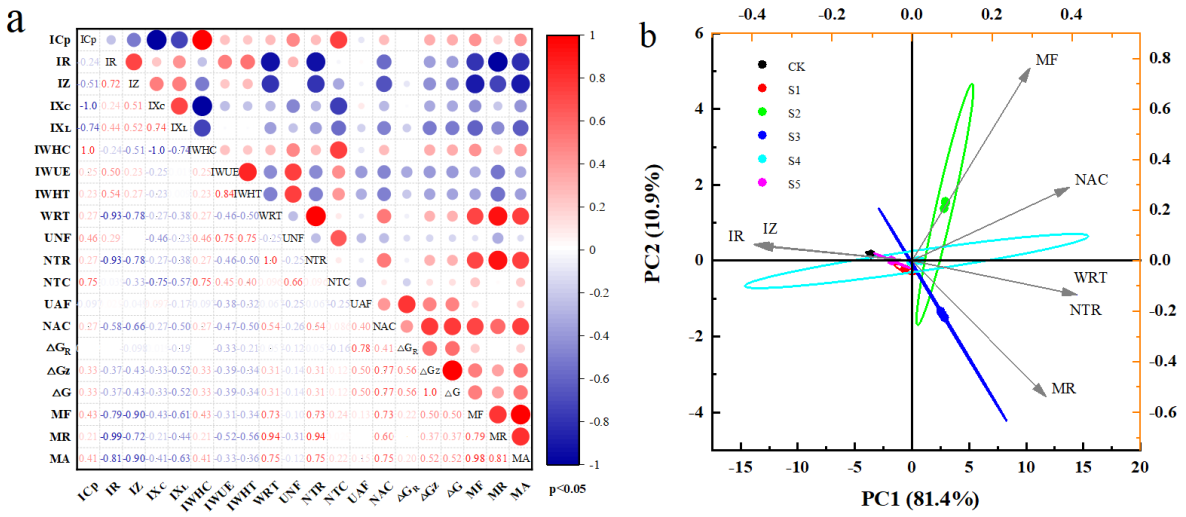

Figure 8. ANOVA (a) and PCA (b) of the electrophysiological nutritional metabolic characteristics of Pb-infected *GBr* leaves under different Se^{4+} treatments.

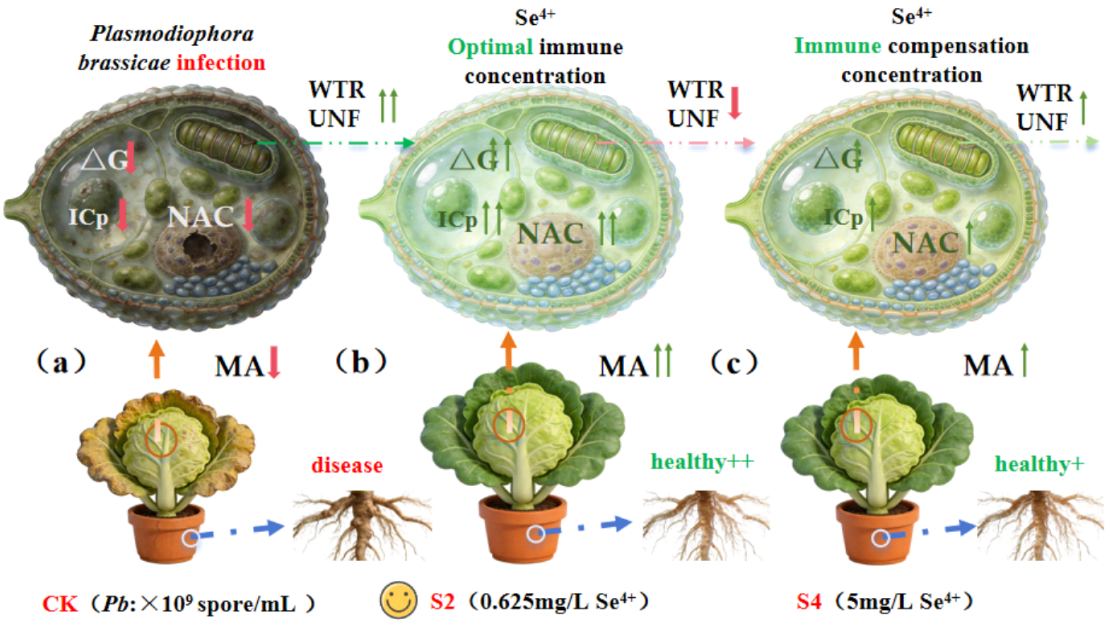

Figure 9. Differential regulation of electrophysiology and immunity of *Pb* infected *GBr* under different Se^{4+} treatments.

4.3 Differential Regulation of Immune Responses to *Pb* Infection in *GBr* by Different Se^{4+} Concentrations

In this study, different Se^{4+} concentrations exerted differential regulatory effects on the immune responses of *GBr* to Pb infection. ANOVA (Figure 8(a)) revealed that the metabolic activity (MA) of *GBr* was significantly positively correlated with WRT, NTR, NAC, MF, and MR, and significantly negatively correlated with IR and IZ, indicating that the electrophysiological metabolic characteristics of *GBr* can be used to explain the differential immune responses [35]. PCA (Figure 8(b)) reveals that the principal components of S1 and S5 are IR and IZ, attributed to S1 and S5 regulating cellular water and nutrient transport by modulating osmotic potentials across the cell membrane [36]; the principal component of S2 is MF, attributed to S2 synergistically promoting ΔG_R and ΔG_Z, thereby enhancing *GBr* cellular metabolic activity [37]; the principal factor for S3 is MR, attributed to S3's synergistic regulation of electrophysiological water transport rate and active nutrient transport capacity in *GBr* [38]; the principal factors for S4 are NAC, WRT, and NTR, attributed to S4's triggering of cellular immune-compensatory metabolism to resist Pb infection [38, 39]. Hence, suitable concentrations of selenite (Se^{4+}) can significantly activate immunity and inhibit clubroot infection in Chinese cabbage, showing good application potential in Enshi high-incidence

areas. Foliar application avoids soil immobilization and improves Se utilization. Combined with rhizosphere probiotics, it prolongs control efficacy, providing a feasible green strategy for clubroot management locally.

5 Conclusion

Based on plant electrophysiological techniques, this study elucidated the differential immune regulation of Pb infection in *GBr* in response to varying Se^{4+} concentrations (Figure 9). Electrophysiological metabolic characteristics revealed that S2 (1.25 mg/L Se^{4+}) is the optimal immune concentration for preventing Pb infection. S2 enhances resistance to Pb infection by synergistically promoting ΔG_R, ΔG_Z, and MA by optimizing electrophysiological water metabolism and nutrient transport. S4 (5 mg/L Se^{4+}) serves as the immune compensation concentration to *GBr*. S4 achieves temporary immune compensation by promoting WRT and NAC, which non-linearly and transiently increase ΔG. In summary, this study provides smart agricultural technology for revealing the electrophysiological immunity to Pb infection of *GBr*.

Data Availability Statement

Data will be made available on request.

Funding

This work was supported in part by the Hubei Minzu University Doctoral Research Startup Project under Grant BS26031; in part by the Hubei Minzu University Graduate Student Research and Innovation Project under Grant MYK2026041; in part by the Enshi Prefecture Science and Technology Program Guided Project under Grant E20230012; in part by the Hubei Province Science and Technology Program Project under Grant 2024BBB082; in part by the Open Fund of the Hubei Provincial Key Laboratory of Selenium Resources Research and Biological Applications under Grant PT10202404.

Conflicts of Interest

The authors declare no conflicts of interest.

AI Use Statement

The authors declare that generative AI tools were used solely for language translation during the preparation of this manuscript. Specifically, DeepL and ChatGPT were employed to assist with the partial translation of content from Chinese into English. All AI-generated translations were carefully reviewed, edited, and verified by the authors to ensure their accuracy, clarity, and consistency with the intended scientific meaning. The authors take full responsibility for the content of this manuscript.

Ethical Approval and Consent to Participate

Not applicable.

References

[1] Liu, W., Dai, Z., Jia, J., Li, X., Zhu, H., Kan, X., & Zhu, B. (2025). Comparative physiological and transcriptomic analyses identify computationally predicted key genes and regulatory pathways in non-heading Chinese cabbage under heat stress. *BMC Plant Biology, 25*(1), 1042. [CrossRef]

[2] Wei, X., Du, Y., Zhang, W., Zhao, Y., Yang, S., Su, H., ... & Yuan, Y. (2024). Comparative metabolome and transcriptome analysis reveals the defense mechanism of Chinese Cabbage (Brassica rapa L. ssp. pekinensis) against plasmodiophora brassicae infection. *International Journal of Molecular Sciences, 25*(19), 10440. [CrossRef]

[3] Ge, W., Lv, M., Feng, H., Wang, X., Zhang, B., Li, K., ... & Ji, R. (2023). Analysis of the role of BrRPP1 gene in Chinese cabbage infected by Plasmodiophora brassicae. *Frontiers in plant science, 14*, 1082395. [CrossRef]

[4] Zhang, Y., Yu, H., Zhao, T., Hussain, I., Ma, X., Wang, Y., ... & Yu, X. (2024). Integrated management of clubroot in zhejiang province, China. *Agronomy, 14*(2), 377. [CrossRef]

[5] Zhu, S., Sun, S., Zhao, W., Yang, X., Mao, H., Sheng, L., & Chen, Z. (2024). Utilizing transcriptomics and proteomics to unravel key genes and proteins of Oryza sativa seedlings mediated by selenium in response to cadmium stress. *BMC Plant Biology, 24*(1), 360. [CrossRef]

[6] Li, Q., Xian, L., Yuan, L., Lin, Z., Chen, X., Wang, J., & Li, T. (2023). The use of selenium for controlling plant fungal diseases and insect pests. *Frontiers in Plant Science, 14*, 1102594. [CrossRef]

[7] Hou, X., Wang, Z., & Peng, M. (2025). Selenium compounds and their bioactivities: molecular mechanisms and prospects for functional food and therapeutic applications. *Plants, 14*(17), 2622. [CrossRef]

[8] Wang, Z., Li, N., Zhou, X., Wei, S., Zhu, Y., Li, M., ... & Cheng, S. (2024). Optimization of fermentation parameters to improve the biosynthesis of selenium nanoparticles by Bacillus licheniformis F1 and its

comprehensive application. *BMC microbiology, 24*(1), 271. [CrossRef]

[9] Zhang, Q., Xing, D., Wu, Y., Zhao, K., Wang, J., & Mao, R. (2024). Effects of Low-Phosphorus Stress on Use of Leaf Intracellular Water and Nutrients, Photosynthesis, and Growth of Brassica napus L. *Horticulturae, 10*(8), 821. [CrossRef]

[10] Yu, R., Wu, Y., & Xing, D. (2021). Can electrophysiological parameters substitute for growth, and photosynthetic parameters to characterize the response of mulberry and paper mulberry to drought?. *Plants, 10*(9), 1772. [CrossRef]

[11] Gu, X., Xia, A., Wu, Y., Gratien, T., Fan, J., Wang, C., ... & Song, X. (2025). Electrophysiological sensors reveal silicon–selenium interaction of dynamic leaf intracellular water–nutrient metabolism in rice under cadmium stress. *Plant Signaling & Behavior, 20*(1), 2547384. [CrossRef]

[12] Xia, A., Wu, Y., Zhai, K., Xiang, D., Li, L., Qin, Z., & Twagirayezu, G. (2025). Plant electrophysiological parameters represent leaf intracellular water–nutrient metabolism and immunoregulations in Brassica rapa during Plasmodiophora infection. *Plants, 14*(15), 2337. [CrossRef]

[13] Kang, H., Lin, Z., Yuan, X., Shi, Y., Xie, X., Li, L., ... & Chai, A. (2024). The occurrence of clubroot in cruciferous crops correlates with the chemical and microbial characteristics of soils. *Frontiers in Microbiology, 14*, 1293360. [CrossRef]

[14] Struck, C., Rüsch, S., & Strehlow, B. (2022). Control strategies of clubroot disease caused by Plasmodiophora brassicae. *Microorganisms, 10*(3), 620. [CrossRef]

[15] Petitpas, M., Lapous, R., Le Duc, M., Lariagon, C., Lemoine, J., Langrume, C., ... & Jubault, M. (2024). Environmental conditions modulate the effect of epigenetic factors controlling the response of Arabidopsis thaliana to Plasmodiophora brassicae. *Frontiers in plant science, 15*, 1245545. [CrossRef]

[16] Zhou, R., Qin, X., Hou, J., & Liu, Y. (2024). Research progress on Brassicaceae plants: a bibliometrics analysis. *Frontiers in Plant Science, 15*, 1285050. [CrossRef]

[17] Sun, S. N., Liu, F., Zeng, L. Y., Chen, W., Ren, L., Xu, L., & Fang, X. P. (2022). Infection process and physiological and biochemical differences between clubroot-resistant and-susceptible varieties of radish. *Chinese Journal of Oil Crop Sciences, 44*(3), 642-651. [CrossRef]

[18] Auer, S., & Ludwig-Müller, J. (2023). Biocontrol of clubroot disease: how successful are endophytic fungi and bacteria?. *European Journal of Plant Pathology, 167*(4), 433-451. [CrossRef]

[19] Majidi, A., Shahhoseini, R., Salehi-Arjmand, H., & Roosta, H. R. (2025). Effect of Hoagland's nutrient solution strengths and sodium silicate on growth, yield and biochemical parameters of Carla (Momordica charantia L.) under hydroponic conditions. *Scientific Reports, 15*(1), 7838. [CrossRef]

[20] Wang, Y., Rao, C., Huang, L., Wu, J., Sun, P., Zhan, J., ... & He, X. (2023). Effects of organic selenium and nanoselenium on drought stress of pak choi (Brassica chinensis var. pekinensis. cv.'Suzhouqing') and its transcriptomic analysis. *Agronomy, 14*(1), 78. [CrossRef]

[21] Khalofah, A., Migdadi, H., & El-Harty, E. (2021). Antioxidant enzymatic activities and growth response of quinoa (Chenopodium quinoa willd) to exogenous selenium application. *Plants, 10*(4), 719. [CrossRef]

[22] Vadillo, J. M., Campillo, C., Millán, S., & Prieto, H. (2025). Evaluation of Nitrogen Nutritional Status in Broccoli, Processing Tomato, and Processing Pepper Under Different Fertilization Regimes in Open Fields in Extremadura. *Horticulturae, 11*(7), 733. [CrossRef]

[23] Wang, L., Zhong, Y., Ma, R., Li, H., & Liu, T. (2025). Comprehensive Evaluation of Phenotypic Traits in Vegetable Faba Bean (Vicia faba L.) Germplasms Based on Multivariate Statistical Methods. *Journal of Food Quality, 2025*(1), 1621073. [CrossRef]

[24] Wang, Y., Sun, P., Nie, M., Zhan, J., Huang, L., Wu, J., ... & Li, X. (2025). Integration of metabolomics and transcriptomics analyses reveals the effects of nano-selenium on pak choi. *Scientific reports, 15*(1), 11215. [CrossRef]

[25] Van Haeverbeke, M., De Baets, B., & Stock, M. (2023). Plant impedance spectroscopy: a review of modeling approaches and applications. *Frontiers in Plant Science, 14*, 1187573. [CrossRef]

[26] Wang, Y., Tan, G., Chen, J., Wu, J., Liu, S., & He, X. (2023). Effects of foliar spraying of organic selenium and nano-selenium fertilizer on pak choi (Brassica chinensis var. pekinensis. cv.'Suzhouqing') under low temperature stress. *Agriculture, 13*(11), 2140. [CrossRef]

[27] Lu, M., Song, Y., & Jin, G. (2025). Trait variation across different life history stages of trees and its impact on net photosynthetic rate. *Frontiers in Plant Science, 16*, 1657142. [CrossRef]

[28] Zhao, Y., & Chen, H. (2025). Water and Nitrogen Use Strategies and Their Influencing Mechanisms in Typical Desert Shrubs of the Qaidam Basin, Qinghai–Tibet Plateau, China. *Plants, 14*(24), 3828. [CrossRef]

[29] Patiño-Ruiz, M. F., Anshari, Z. R., Gaastra, B., Slotboom, D. J., & Poolman, B. (2024). Chemiosmotic nutrient transport in synthetic cells powered by electrogenic antiport coupled to decarboxylation. *Nature Communications, 15*(1), 7976. [CrossRef]

[30] An, L., Mao, Y., Huang, D., Leng, Y., & Chen, X. (2025). Selenium in tea plant cultivation: bioavailability, uptake, metabolism, and physiological regulation. *Frontiers in Plant Science, 16*, 1718992. [CrossRef]

[31] Sun, P., Ge, G., Sun, L., Bao, J., Zhao, M., Hao, J., ... & Jia, Y. (2025). Metabolomics combined with physiology and transcriptomics reveal the regulation of key nitrogen metabolic pathways in alfalfa by foliar spraying with nano-selenium. *Journal of Nanobiotechnology, 23*(1), 7. [CrossRef]

[32] Deng, C. L., Liang, Y. E., Liao, J. Y., Lan, J. S., Saito, M. W., Chen, Y. X., ... & Zhan, X. J. (2025). Foliar application of chelated selenium modulated the chlorophyll metabolism, antioxidant capacity, and yield of rice under salt stress. *American Journal of Plant Sciences, 16*(5), 608–620. [CrossRef]

[33] Tangjaidee, P., Swedlund, P., Xiang, J., Yin, H., & Quek, S. Y. (2023). Selenium-enriched plant foods: Selenium accumulation, speciation, and health functionality. *Frontiers in Nutrition, 9*, 962312. [CrossRef]

[34] Khan, Z., Thounaojam, T. C., Chowdhury, D., & Upadhyaya, H. (2023). The role of selenium and nano selenium on physiological responses in plant: a review. *Plant Growth Regulation, 100*(2), 409-433. [CrossRef]

[35] Ullah, S., & Junjun, N. (2026). From signals to survival: exploring chemical, electrical, and acoustic communication mechanisms in plant adaptation to environmental stressors. *Plant and Soil, 518*(2), 1921-1946. [CrossRef]

[36] Yadav, S., Sharma, S., Sharma, K. D., Dhansu, P., Devi, S., Preet, K., ... & Kumar, A. (2023). Selenium mediated alterations in physiology of wheat under different soil moisture levels. *Sustainability, 15*(3), 1771. [CrossRef]

[37] Samynathan, R., Venkidasamy, B., Ramya, K., Muthuramalingam, P., Shin, H., Kumari, P. S., ... & Sivanesan, I. (2023). A recent update on the impact of nano-selenium on plant growth, metabolism, and stress tolerance. *Plants, 12*(4), 853. [CrossRef]

[38] Mechora, Š., Stibilj, V., Kreft, I., & Germ, M. (2014). The physiology and biochemical tolerance of cabbage to Se (VI) addition to the soil and by foliar spraying. *Journal of plant nutrition, 37*(13), 2157-2169. [CrossRef]

[39] Xia, A., Wu, Y., Qin, Z., Zhu, Y., Li, L., Xiao, J., ... & Xiang, J. (2024). Synergistic effects of bicarbonate and selenium on cadmium transport in karst-adaptable plants based on plant electrical signals. *Agronomy, 14*(1), 218. [CrossRef]

Antong Xia is a postdoctor candidate in geochemistry at the University of Chinese Academy of Sciences, Institute of Geochemistry (Guiyang, China), integrating stable-isotope geochemistry, plant electrical biotechnology to explore the internal physiological status of mangrove leaf cells. Previously, Phd.Xia is a lecturer at Hubei Minzu University (Enshi, China). Affiliated organization: School of Chemical and Environmental Engineering, Hubei Minzu University, Enshi, China. (Email: xiaantong@hbmzu.edu.cn)

Huakang Huang is studying at Hubei Minzu University.Affiliated organization: School of Chemical and Environmental Engineering, Hubei Minzu University, Enshi, China. (Email: 2795940985@qq.com)

Nan Mou is currently an undergraduate student majoring in Environmental Science at the School of Chemical and Environmental Engineering, Hubei Minzu University, Enshi, China. (Email: 202312424@hbmzu.edu.cn)

Jing Fan received the bachelor of Science degree in Biological Sciences from Hubei Minzu University in China in 2024. She is currently affiliated with the School of Chemical and Environmental Engineering, Hubei Minzu University, Enshi, China. (Email: 202430385@hbmzu.edu.cn)

Kun Zhai received her M.S. degree in Soil Science from Guizhou University in 2005, and her Ph.D. degree in Soil Science from Huazhong Agricultural University in 2015. She is currently a Professor and Master's Supervisor at the School of Chemical and Environmental Engineering, Hubei Minzu University, Enshi, China. Her research interests include soil pollution remediation and soil environmental chemistry. She has hosted or participated in more than 10 research projects, published over 10 SCI/EI papers as first or corresponding author, and obtained 1 authorized national invention patent. (Email: zk3100@sina.com)

Dongshan Xiang received his M.S. degree in Plant Nutrition from Guizhou University in 2005, and his Ph.D. degree in Analytical Chemistry from Wuhan University in 2012. He is currently a Professor and Master's Supervisor at the School of Chemical and Environmental Engineering, Hubei Minzu University, Enshi, China. His research interests include molecular fluorescence analysis and soil heavy metal analysis. He has hosted or participated in multiple national and provincial research projects, published over 20 SCI/EI academic papers as first or corresponding author, and obtained 1 authorized national invention patent. (Email: zk3100@sohu.com)